Electron Paramagnetic Resonance Studies of Metalloporphyrin Anion Radicals. Effects of Solvent, Counterion, Temperature, and Isotopic Substitution on the Jahn-Teller Active ^2E_g Ground State

Jyoti Seth and David F. Bocian*

Contribution from the Department of Chemistry, University of California, Riverside, California 92521

*Received July 26, 1993**

Abstract: Electron paramagnetic resonance (EPR) spectra are reported for a series of porphyrin anion radicals including H_2TPP^-, H_2OEP^-, $MgTPP^-$, $ZnTPP^-$, $ZnOEP^-$, and $CdTPP^-$ (TPP = tetraphenylporphyrin, OEP = octaethylporphyrin). The anions were generated by both chemical and electrochemical reduction in a variety of solvents. EPR spectra are also reported for a number of isotopomers of the free bases and Zn(II) complexes. These isotopomers included TPP-β-d_8, TPP-(*meso*-^{13}C)$_4$, TPP-(^{15}N)$_4$, and OEP-*meso*-d_4. The temperature dependence of the EPR spectra was also investigated from 6 to 380 K. Contrary to previous reports, the spectra are not particularly sensitive to the solvent or counterion. The low-temperature spectra of all the anion radicals are anisotropic with $g_\parallel < g_e$. The anisotropy for H_2TPP^- (and H_2OEP^-) and $MgTPP^-$ is small ($\sim$0.0003 and $\sim$0.0023, respectively). On the other hand, the anisotropy is significant for $ZnTPP^-$ (and $ZnOEP^-$) and $CdTPP^-$ ($\sim$0.01 and $\sim$0.02, respectively). The anisotropic EPR spectra are indicative of unquenched orbital angular momentum in the ground states of the anion radicals. The EPR spectra were modeled by using an harmonic potential function which is subject to both Jahn-Teller and strain distortions. The general characteristics of the spectra are well accounted for by a model that assumes distortions along a single vibronically active coordinate. However, the detailed characteristics of the EPR line shape indicate that more than one mode is involved. Simulations of the EPR spectra indicate that the Jahn-Teller energy is less than the zero point energy of the active vibrational modes; accordingly, the distortion is dynamic rather than static. The calculations, in conjunction with the spectral data, indicate that the strain energy is substantial (at least 100 cm^{-1}) in both the solid and liquid states. The strain distortion alters the relative energies of the two wells in the Jahn-Teller distorted system. Accordingly, the dynamically averaged structure does not have rigorous 4-fold symmetry.

Introduction

Tetrapyrrolic macrocycles undergo successive one-electron reductions leading to mono-, di-, and trianions.[1] Monoanionic species serve as intermediates in the early events of photosynthesis.[2,3] The importance of anion radicals in photosynthesis has led to a long standing interest in their structural and electronic properties.[4-6] Electron paramagnetic resonance (EPR) spectroscopy has been used extensively to characterize the anion radicals of photosynthetic pigments and model compounds ((bacterio)chlorins,(bacterio)chlorophylls,and(bacterio)pheophytins).[1,7,8] These compounds differ structurally from porphyrins in that one (or two) of the pyrrole rings is (are) saturated and a fifth isocyclic ring is part of the structure (photosynthetic pigments).[9] Surprisingly, only a few EPR studies have been reported for the anion radicals of the parent porphyrin and metalloporphyrin compounds.[1,10-17] Most of these latter studies were conducted a number of years ago and were fairly limited in scope. Early EPR studies of porphyrinic anions focused primarily on *meso*-tetraphenylporphyrin (H_2TPP^-) and its Zn(II) complex ($ZnTPP^-$).[10,12,14-16] Spectra of both chemically and electrochemically generated H_2TPP^- and $ZnTPP^-$ have been reported in several solvents at ambient and low temperatures (77 K). EPR spectra have also been reported for $MgTPP^-$, $CdTPP^-$, and the anions of several β-substituted porphyrins (free base and Mg(II) deuteroporphyryin; Mg(II) protoporphyrin; Zn(II) and Mg(II) etioporphyrin).[12,13,16] With a single exception,[13b] these spectra were recorded at room temperature in a single solvent. None of the above studies utilized isotopically substituted porphyrins or examined the temperature dependence of the EPR spectra. The limited amount of EPR data available for porphyrinic anions has precluded a thorough analysis of the spectra or the detailed characterization of the electronic ground state.

The EPR spectra reported for H_2TPP^- and the anion radicals of other free base porphyrins are generally characteristic of organic radicals. H_2TPP^- exhibits an isotropic signal at g $\sim$ 2.0026 with a peak-to-peak line width of $\sim$5 G at both room and low temperatures.[12,14,16] No hyperfine structure is observed. In the case of $ZnTPP^-$, significant variations in the g values and line widths have been reported under different conditions. Several groups have reported a broad signal (20-25 G) with no hyperfine structure at room temperature.[10,12,15] This signal was observed for both chemically and electrochemically generated $ZnTPP^-$ in different solvents. One of these studies reported g = 2.0025,[15]

* Abstract published in *Advance ACS Abstracts,* December 1, 1993.

(1) Fajer, J.; Davis, M. S. In *The Porphyrins*; Dolphin, D., Ed.; Academic Press: New York, 1979; Vol. IV, pp 197-256.
(2) Kirmaier, C.; Holten, D. *Photosynth. Res.* **1987**, *13*, 225-260.
(3) Parson, W. W. In *Chlorophylls*; Scheer, H., Ed.; CRC Press: Boca Raton, FL, 1991; pp 1153-1180.
(4) Gurinovich, G. P.; Gurinovich, I. F.; Ivashin, N. V.; Sinyakov, G. N.; Shulga, A. M.; Terekhov, S. N.; Filatov, I. V.; Dzilinski, K. *J. Mol. Struct.* **1988**, *172*, 317-343.
(5) Hansen, L. K. In ref 3, pp 993-1014.
(6) Plato, M.; Möbius, K.; Lubitz, W. In ref 3, pp 1015-1046.
(7) Lubitz, W. In ref 3, pp 903-944.
(8) Angerhofer, A. In ref 3, pp 945-991.
(9) Jones, O. T. G. In *The Porphyrins*; Dolphin, D., Ed.; Academic Press: New York, 1979; Vol. VI, pp 179-232.
(10) Closs, G. L.; Closs, L. E. *J. Am. Chem. Soc.* **1963**, *85*, 818-819.
(11) Dodd, J. W.; Hush, N. S. *J. Chem. Soc.* **1964**, 4607-4612.
(12) Felton, R. H.; Linschitz, H. *J. Am. Chem. Soc.* **1966**, *88*, 1113-1116.
(13) (a) Hush, N. S.; Rowlands, J. R. *J. Am. Chem. Soc.* **1967**, *89*, 2976-2979. (b) Bobrovskii, A. P.; Kholgorov, V. Ye. *Biofizika* **1974**, *19*, 50-55.
(14) Peychal-Heiling, G.; Wilson, G. S. *Anal. Chem.* **1971**, *43*, 550-556.
(15) Kholmogorov, V. E.; Maslov, V. G. *Opt. Spectrosc.* **1971**, 195-199.
(16) Lexa, D.; Reix, J. *Chim. Phys. Physicochim. Biol.* **1974**, *71*, 517-524.
(17) Donohoe, R. J.; Atamian, M.; Bocian, D. F. *J. Am. Chem. Soc.* **1987**, *109*, 5593-5599.

0002-7863/94/1516-0143$04.50/0

near the free electron value (g_e), whereas another reported g = 2.0000,[12] substantially below g_e. On the other hand, a different study reported that ZnTPP$^-$ exhibits a relatively narrow line (~5 G) at g = 2.0025 at room temperature.[16] The only low-temperature (77 K) EPR study of ZnTPP$^-$ reported that the chemically generated anion exhibits a relatively narrow line (7–10 G) at g = 2.0025.[15]

The large variations observed in the EPR spectra of ZnTPP$^-$ under different conditions have generally been attributed to the fact that metalloporphyrin anions have an orbitally degenerate ^2E_g ground electronic state (D_{4h} symmetry) which is subject to both static and dynamic Jahn–Teller distortions.[1] Several reports have placed the Jahn–Teller energy in the 70–200-cm^{-1} range.[12,18] These energies are at or below the thermal energy at which the various EPR experiments were performed. Accordingly, the detailed features of the EPR spectrum (hyperfine structure, line width, and line shape) might be extremely sensitive to the solvent, temperature, and/or counterion due to dynamical effects. The fact that the EPR spectrum of H_2TPP^- is not sensitive to these experimental parameters lends credence to this argument. The ground state of this latter ion is an orbital singlet, B_{2g} or B_{3g} (D_{2h} symmetry), which is not subject to Jahn–Teller instability.[19] On the other hand, CdTPP$^-$, which is subject to Jahn–Teller effects, has been reported to exhibit EPR features more similar to H_2TPP^- than to ZnTPP$^-$.[12] Finally, it must be noted that a number of workers have cautioned that the EPR features attributed to metalloporphyrin anion radicals might be due instead to impurities, either found in the solvents or generated during the course of the reduction.[1,10,13a]

The limited amount of EPR data available for metalloporphyrin anion radicals along with the inconsistencies in the spectra reported for ZnTPP$^-$ and CdTPP$^-$ prompted us to carry out a detailed, systematic EPR study of a series of these anion radicals. These species included MgTPP$^-$, ZnTPP$^-$, CdTPP$^-$, and ZnOEP$^-$ (OEP = octaethylporphyrin). The EPR spectra of the parent free bases H_2TPP^- and H_2OEP^- were also obtained for comparison. The various anions were generated by both chemical (sodium amalgam) and electrochemical (bulk electrolysis) reductions in a variety of solvents. In the course of these studies, EPR spectra were obtained for a number of isotopomers of the free base and Zn(II) complexes. These included TPP-β-d_8, TPP-(*meso*-^{13}C)$_4$, TPP-(^{15}N)$_4$, and OEP-*meso*-d_4. Finally, the temperature dependence of the EPR spectra was investigated from 6 to 380 K. Collectively, these studies reveal for the first time the true features of the EPR spectra of the metalloporphyrin monoanion radicals and provide new insights into the nature of the Jahn–Teller active ^2E_g ground state.

Experimental Section

H_2TPP (chlorin free) and H_2OEP were obtained from Midcentury and used as received. H_2TPP-(^{15}N)$_4$ and H_2TPP-(*meso*-^{13}C)$_4$ were prepared as described by Lindsey et al. by using the appropriate pyrrole (pyrrole, Aldrich; pyrrole-^{15}N, MSD Isotopes, 99.3% isotopic purity) and benzaldehyde (benzaldehyde, Aldrich; benzaldehyde-α-^{13}C, MSD Isotopes, 99.9% isotopic purity).[20] H_2TPP-β-d_8 was synthesized as described by Shirazi and Goff.[21] H_2OEP-*meso*-d_4 was prepared by standard procedures.[22] MgTPP, ZnTPP, and ZnOEP (and the various isotopomers of the Zn(II) complexes) were prepared by using the DMF method.[23] The Mg(II) complex was obtained from the chloride salt; the Zn(II) complexes were obtained from the acetate salt. The TPP and OEP complexes were purified on basic alumina and $MgCO_3$ columns, respectively, by using CH_2Cl_2 as the eluting solvent. CdTPP was synthesized from the acetate salt by using the procedure described by Hudson and Smith for the preparation of HgTPP.[24]

The anions of the normal isotopomers of the various compounds were prepared by both chemical and electrochemical techniques. The anions of the isotopically labeled species were prepared only by the latter method. All reductions were conducted in a Vacuum Atmospheres glovebox (Model HE-93) equipped with a Dri-Train (Model 493). The chemical reductions were performed by placing the sample in an EPR tube containing a 1% sodium amalgam. The electrochemical reductions were conducted in a standard three compartment cell by using electrochemical instrumentation described elsewhere.[17] Subsequent to reduction, the samples were transferred to a flat cell or standard EPR tube and sealed in the glove box. [The low-temperature spectra of the chemically reduced species were obtained in the same EPR tube used for the reduction.] The room temperature EPR spectra were acquired no more than 15 min after generating the anions. The samples used in the low-temperature experiments were immediately frozen at 77 K and maintained at that temperature until use. All solvents used for the chemical and electrochemical reductions were obtained from Aldrich and purified by standard procedures. Tetrahydrofuran (THF) was purified by using sodium and benzophenone. *N*,*N*′-Dimethylformamide (DMF) was stored over 4-Å molecular sieves for several weeks and distilled from basic alumina *in vacuo*. Butyronitrile (BuN) was purified by using the method of Van Duyne and Reilley.[25] Prior to use, all solvents were degassed thoroughly by the freeze–pump–thaw technique. The supporting electrolyte used for all the electrochemical reductions was ~0.1 M tetrabutylammonium hexafluorophosphate (Aldrich, recrystallized three times from absolute ethanol and dried at 110 °C *in vacuo*).

The integrity of the anions was confirmed by absorption spectroscopy for the chemically reduced species and by cyclic voltammetry, coulometry, and absorption spectroscopy for the electrochemically reduced species. These measurements revealed that all the compounds yield reduced species reasonably free of decomposition products with the exception of CdTPP$^-$. Both cyclic voltammetry and absorption spectroscopy revealed that this latter complex was contaminated by H_2TPP^-. The free base impurity is formed during the reduction process. The EPR signal from H_2TPP^- is much narrower than that of CdTPP$^-$ and dominates the spectrum if low concentrations of neutral ($<5 \times 10^{-4}$ M) are used for the reduction (vide infra).

The EPR spectra were recorded on a Bruker ER 200D X-band spectrometer. Temperature control was achieved by using an Oxford Instruments ESR 900 continuous flow He cryostat (5–120 K) or a Bruker continuous flow N_2 cryostat (100–280 K). Spectra required at 77 K were obtained by using a liquid N_2 finger Dewar. The g values were measured with a Bruker ER 035M NMR gauss meter and a Hewlett-Packard 3550B microwave frequency counter. The accuracy of the g values was assessed from the known value of DPPH[26a] and was determined to be ±0.0002 unless otherwise noted.

Results

A. TPP Complexes. Representative EPR spectra of H_2TPP^-, MgTPP$^-$, ZnTPP$^-$, and CdTPP$^-$ obtained at 300, 77, and 10 K are shown in Figure 1. The spectra of the different isotopomers of H_2TPP^- and ZnTPP$^-$ obtained under the same conditions are shown in Figures 2 and 3, respectively. The spectral parameters for the various anions are summarized in Table 1. The values of g_{av} were measured from the zero crossing points in the 300 K spectra; the values of a_{av} were obtained from computer simulations of these spectra. The values of $g_\parallel$, $g_\perp$, $a_\parallel$, and $a_\perp$ were obtained from simulations of the 77 K spectra. The specific features of the EPR spectra of the different anions are described in more detail below. Prior to this discussion, it is useful to describe the results of the studies in which different solvents and/or reduction procedures were used to generate the anion radicals.

The EPR spectra shown in Figures 1–3 were obtained from electrochemically generated anions in BuN. For comparison,

(18) Maslov, V. G. *Opt. Spectrosc.* **1974**, *37*, 580–581.
(19) Gouterman, M. In *The Porphyrins*; Dolphin, D., Ed.; Academic Press: New York, 1978; Vol. III, pp 1–165.
(20) (a) Lindsey, J. S.; Hsu, H. C.; Schreiman, I. C. *Tetrahedron. Lett.* **1986**, *27*, 4969–4970. (b) Lindsey, J. S.; Schreiman, I. C.; Hsu, H. C.; Kearney, P. C.; Marguerettaz, A. M. *J. Org. Chem.* **1987**, *52*, 827–836.
(21) Shirazi, A.; Goff, H. M. *J. Am. Chem. Soc.* **1982**, *104*, 6318–6322.
(22) Bonnett, R.; Gale, I. A. D.; Stephenson, G. F. *J. Chem. Soc. C* **1967**, 1168–1172.
(23) Alder, A. D.; Longo, F. R.; Kampas, F.; Kim, J. *J. Inorg. Nucl. Chem.* **1970**, *32*, 2443–2445.
(24) Hudson, M. F.; Smith, K. M. *Tetrahedron* **1976**, *32*, 597–601.
(25) Van Duyne, R. P.; Reilley, C. N. *Anal. Chem.* **1972**, *44*, 142–152.
(26) (a) Wertz, J. E. Bolton, J. R. *Electron Spin Resonance: Elementary Theory and Practical Applications*; McGraw-Hill: New York, 1972; p 465. (b) *Ibid.* pp 71–72.

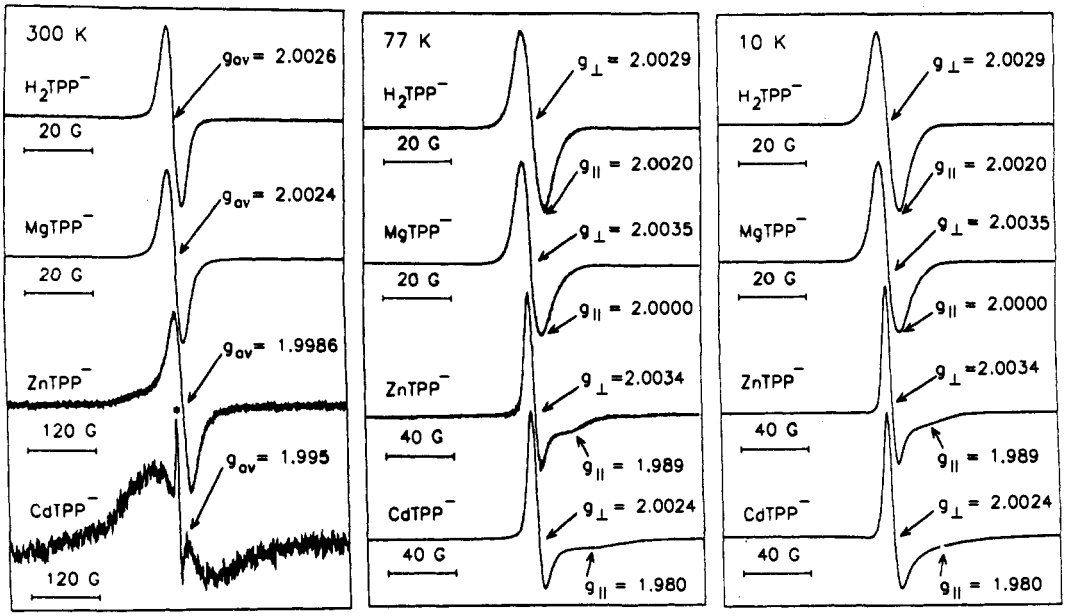

Figure 1. EPR Spectra of electrochemically generated H_2TPP^-, $MgTPP^-$, $ZnTPP^-$, and $CdTPP^-$ in BuN at 300, 77, and 10 K. The signal marked by the asterisk in the 300 K spectrum of $CdTPP^-$ is due to a TPP^- impurity (see text).

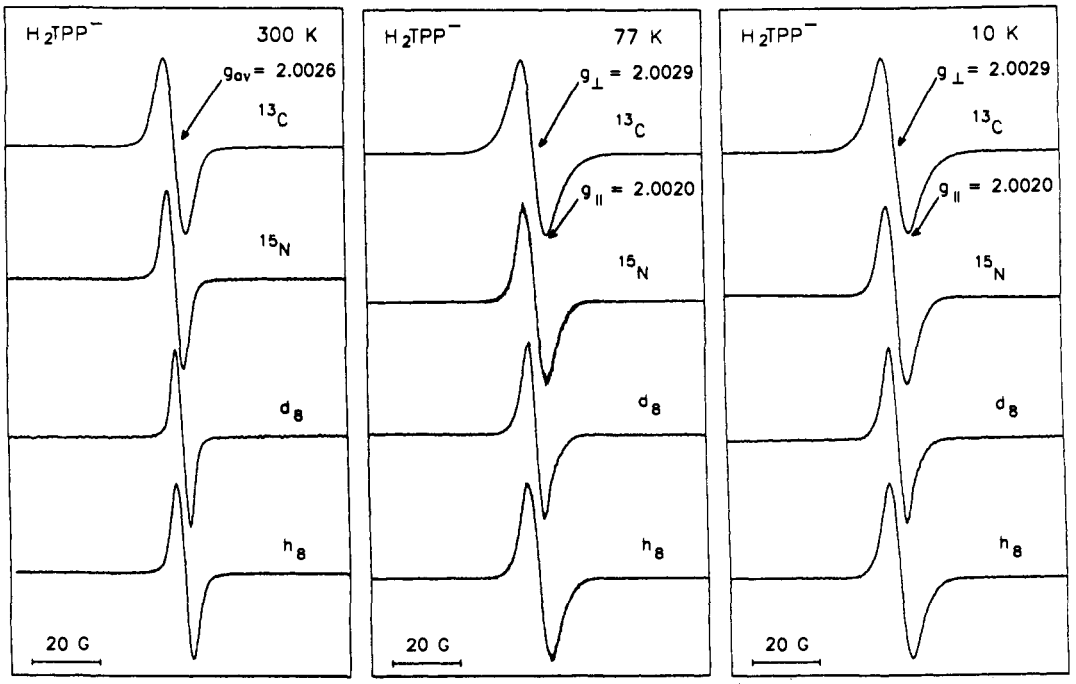

Figure 2. EPR spectra of electrochemically generated H_2TPP^-, $[H_2TPP\text{-}\beta\text{-}d_8]^-$, $[H_2TPP\text{-}(^{15}N)_4]^-$, and $[H_2TPP\text{-}(meso\text{-}^{13}C)_4]^-$ in BuN at 300, 77, and 10 K.

the spectra of $ZnTPP^-$ obtained at 300, 77, and 20 K in BuN, THF, and DMF are shown in Figure 4. As can be seen, the spectra of $ZnTPP^-$ are similar in the three solvents at a given temperature. This was also found to be the case for the other anions (spectra not shown). EPR spectra were also obtained for chemically generated anions of the various metalloporphyrin complexes at ambient and low temperatures in BuN, THF, and DMF (not shown). [Chemical reduction of H_2TPP yields Na_2TPP^-.[11]] These spectra were found to be essentially identical to those shown in Figures 1 and 3. In no instance was any evidence found for ion pairing (such as the observation of ^{23}Na hyperfine structure).[26b] In certain instances, EPR signals different from those shown in the figures were observed; however, these spectral features only occurred when the solvent was not rigorously dried and purified. The spurious signals were observed more frequently when chemical reduction was used to generate the anions. This is most likely due to the fact that this process is more difficult to control than electrochemical reduction. Collectively, our results suggest that the general features of the EPR spectra of the metalloporphyrin anion radicals are not particularly sensitive to the type of solvent or the nature of the counterion and that previous reports to the contrary are in error.

1. TPP^- and $MgTPP^-$. The EPR spectra of H_2TPP^- and $MgTPP^-$ are similar to one another at both ambient and low temperatures. At ambient temperatures, both anions exhibit symmetrical narrow lines ($\sim$5 G) at $g_{av} \approx 2.0025$. These results are consistent with those of previous EPR studies.[12,14,16] At low temperatures, the EPR signals from H_2TPP^- and $MgTPP^-$ are anisotropic and characteristic of an axially symmetric spin system. [In the case of H_2TPP^-, the axial symmetry must result from accidental degeneracy because the complex has D_{2h} symmetry.] In case of H_2TPP^-, the anisotropy is very small ($g_\parallel$ = 2.0020, $g_\perp$ = 2.0029) and hardly observable. In the case of $MgTPP^-$, the anisotropy is sufficiently large ($g_\parallel$ = 2.0000, $g_\perp$ = 2.0035) that

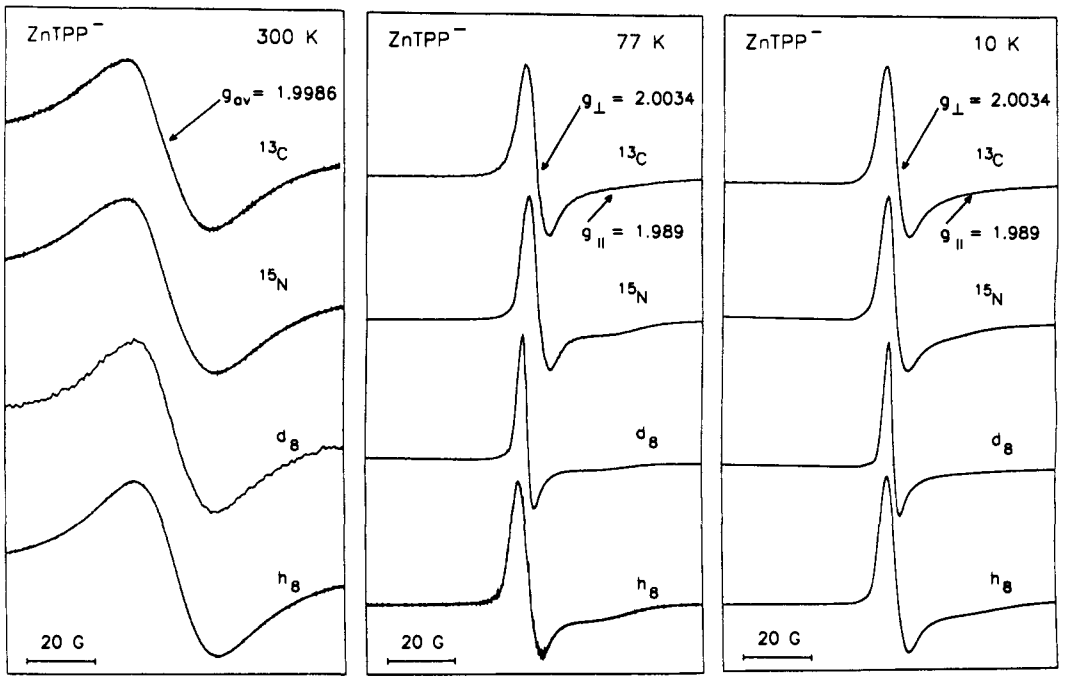

Figure 3. EPR spectra of electrochemically generated ZnTPP⁻, [ZnTPP-β-d_8]⁻, [ZnTPP-(^{15}N)$_4$]⁻, and [ZnTPP-(*meso*-^{13}C)$_4$]⁻ in BuN at 300, 77, and 10 K.

Table 1. EPR Parameters for the Anion Radicals

	g_{av}[a]	$g_\parallel$[b]	$g_\perp$[b]	a_{av} (G)[a]	$a_\parallel$ (G)[b]	$a_\perp$ (G)[b]	ΔH (G)[a]
TPP⁻	2.0026	2.0020	2.0029	1.9 (β-h)	1.1	2.2	4.5
[TPP-β-d_8]⁻	2.0026	2.0020	2.0029	0.28 (β-*d*)	0.18	0.34	3.5
[TPP-(^{15}N)$_4$]⁻	2.0026	2.0020	2.0029	*c*	*c*	*c*	4.5
[TPP-(*meso*-^{13}C)$_4$]⁻	2.0026	2.0020	2.0029	2.5 (*meso*-^{13}C)	6.1	0.71	6.3
MgTPP⁻	2.0024	2.0000	2.0035	0.93 (β-*h*)	0.57	1.1	4.8
ZnTPP⁻	1.9986	1.989	2.0034	0.93 (β-*h*)	0.57	1.1	26
[ZnTPP-β-d_8]⁻	1.9986	1.989	2.0034	0.14 (β-*d*)	0.087	0.17	26
[ZnTPP-(^{15}N)$_4$]⁻	1.9986	1.989	2.0034	*c*	*c*	*c*	26
[ZnTPP-(*meso*-^{13}C)$_4$]⁻	1.9986	1.989	2.0034	2.5 (*meso*-^{13}C)	6.1	0.71	26
CdTPP⁻	1.995	1.980	2.0024	0.93 (β-*h*)	0.57	1.1	120
OEP⁻	2.0027	2.0021	2.0030	2.73 (*meso*-*h*)	1.8	3.2	5.8
[OEP-(*meso*-d_4)]⁻	2.0027	2.0021	2.0030	0.42 (*meso*-*d*)	0.28	0.49	2.8
ZnOEP⁻	1.9994	1.989	2.0027	2.73 (*meso*-*h*)	1.8	3.2	18
[ZnOEP-(*meso*-d_4)]⁻	1.9994	1.989	2.0027	0.42 (*meso*-*d*)	0.28	0.49	18

[a] Values obtained from the 300 K spectra. g_{av} was measured at the zero crossing point; the accuracy of these values is ±0.0002 except for that of CdTPP⁻, which is ±0.001. a_{av} was obtained from simulations of the spectra using a Gaussian line shape with a full width at half-maximum (FWHM) = 1.86 G. ΔH is the peak-to-peak width. [b] Values obtained from simulations of the 77 K spectra using a Gaussian line shape with a FWHM ≈ 2.0 G ($\perp$) and ≈ 6.5 G ($\parallel$). The $g_\parallel$ values listed for ZnTPP⁻ and CdTPP⁻ are those at the maximum of the distribution required to fit the spectrum; the accuracy of these values is ±0.001 (see text). [c] The hyperfine parameters for nitrogen are very small (<1 g) and could not be estimated from the isotopic substitutions.

the line shape is clearly asymmetric. The slight asymmetry in the EPR signal for H_2TPP^- has been noted in a previous low-temperature EPR study.[15] There have been no previous low-temperature EPR studies of MgTPP⁻. The anisotropic line shapes observed for the two anion radicals are indicative of unquenched orbital angular momentum in the electronic ground states.

The EPR spectra of the different isotopomers of H_2TPP^- fail to reveal any resolved hyperfine structure at either ambient or low temperature (Figure 2). However, the line width of the EPR signal for [H_2TPP-β-d_8]⁻ is distinctively narrower than that for H_2TPP^-, whereas the line width for [H_2TPP-(*meso*-^{13}C)$_4$]⁻ is significantly broader. The different line widths observed for the isotopomers reflect contributions from unresolved hyperfine structure. On the other hand, the line widths for H_2TPP^- and [H_2TPP-($^{15}N_4$)]⁻ are essentially identical. The hyperfine couplings for the β-hydrogen and *meso*-^{13}C atoms can be estimated by using the line width observed for [H_2TPP-β-d_8]⁻ as a reference. Simulations of the ambient temperature spectra indicate that $a_{av}(\beta\text{-}h) \approx 1.9$ G and $a_{av}(^{13}C) \approx 2.5$ G. Simulations of the low-temperature spectra indicate that $a_\parallel(\beta\text{-}h) \approx 1.1$ G and $a_\perp(\beta\text{-}h) \approx 2.2$ G; $a_\parallel(^{13}C) \approx 6.1$ G and $a_\perp(^{13}C) \approx 0.71$ G. At all temperatures $a_{av}(^{14}N/^{15}N) < 1$ G. These values assume contributions from four β-hydrogen, four *meso*-^{13}C, and two pyrrole $^{14}N/^{15}N$ atoms. Only four of the eight β-hydrogen atoms contribute significant hyperfine structure because the β-carbon spin density is localized on two of the four pyrrole rings in the D_{2h} complex.[1,12] Likewise, the spin density is localized on only two of the four pyrrole nitrogen atoms; however, these atoms are on the other pair of pyrrole rings. Application of the McConnell relation results in spin densities of ~0.1, ~0.7, and <0.03 on the *meso*-carbon, β-carbon, and pyrrole nitrogen atoms, respectively.[27] These values are consistent with the results of molecular orbital calculations which predict the spin densities on these three types of atoms to be 0.083, 0.066, and 0.053, respectively.[1,12]

2. ZnTPP⁻. The EPR spectra of ZnTPP⁻ are distinctly different from those of H_2TPP^- and MgTPP⁻ (Figure 1). At ambient temperatures, the EPR signal from ZnTPP⁻ is very broad (~26 G) and centered at $g_{av} = 1.9986$. This line width is similar to that reported in several (but not all) previous studies.[10,12,15] In contrast, the value of g_{av} determined from our spectra is lower

(27) These values were calculated by using $a_i = Q_i\rho_C$ with $Q_H = -25$ G and $Q_C = 25$ G (see ref 1).

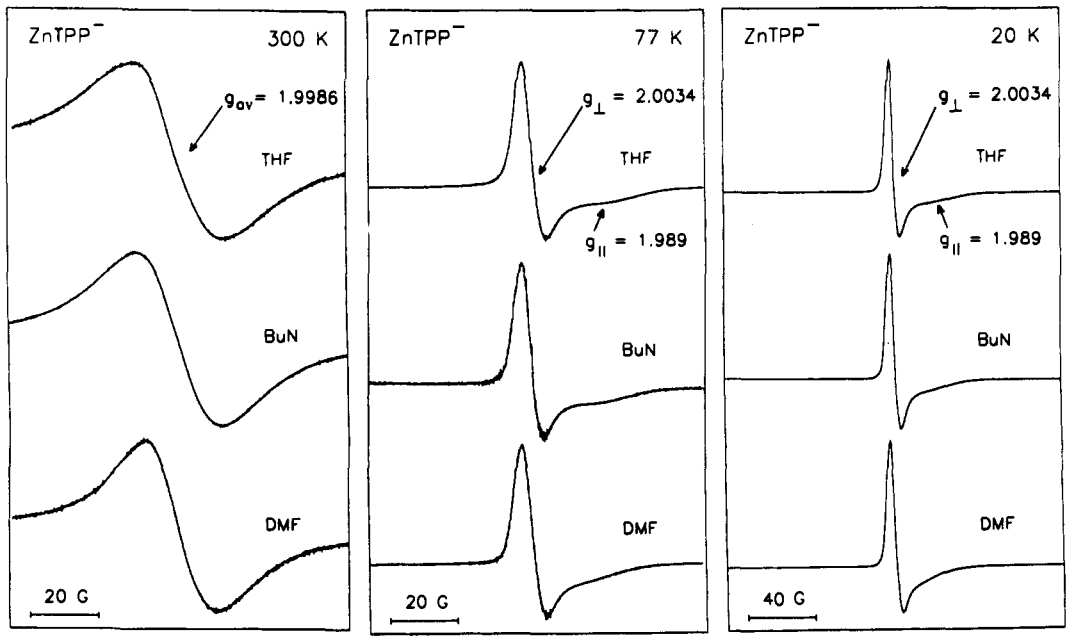

Figure 4. EPR spectra of electrochemically generated ZnTPP⁻ in THF, BuN, and DMF at 300, 77, and 20 K.

than any of the previously reported values and significantly less than g_e. In addition, the line shape we observe is distinctly asymmetric and poorly represented by either a single Gaussian or Lorentzian function. [An earlier EPR study reported that the line shape was approximately Lorentzian.[12]] Computer simulations indicate that the band contour of ZnTPP⁻ can be fit with multiple Gaussian or Lorentzian lines; however, no unique fit is possible.

The low-temperature EPR spectrum of ZnTPP⁻ is different from the ambient-temperature spectrum (Figure 1). As was reported in an earlier study, the low-temperature spectrum is characterized by a narrow (~10 G) asymmetrical feature near g_e rather than a broad signal.[15] However, closer examination of the low-temperature spectrum reveals a second much broader (20–30 G) feature centered near g = 1.989. This feature was apparently overlooked in the previous low-temperature EPR study of ZnTPP⁻. Together the narrow and broad features are indicative of an axially symmetric spin system with $g_\parallel$ = 1.989 and $g_\perp$ = 2.0034 (Table 1). The observation of an anisotropic low-temperature spectrum for ZnTPP⁻ is consistent with the EPR features exhibited by H_2TPP⁻ and MgTPP⁻; however, the anisotropy for the former anion is significantly larger than for either of the latter (vide supra). The low $g_\parallel$ value observed for ZnTPP⁻ is also consistent with the low g_{av} value seen at ambient temperatures.

Simulations of the low-temperature EPR spectrum of ZnTPP⁻ revealed that no combination of g values, hyperfine parameters, or line widths could satisfactorily reproduce the observed band contour. Reasonable fits could only be obtained if the broad $g_\parallel$ feature was represented as a distribution of narrower overlapping signals whose relative intensities were not described by any analytical distribution function. This is illustrated in Figure 5, which shows a series of independent spectral components whose sum gives a reasonable fit to the 10 K EPR spectrum of ZnTPP⁻. In this simulation, the line widths for the different $g_\parallel$ components were chosen to be the same as those of the narrow $g_\perp$ features. These latter features were given identical $g_\perp$ values. With this choice of line widths for the $g_\parallel$ signals, components as low as 1.98 must be included to account for the intensity in the high-field wing of the spectrum. Obviously, this fit is not unique; however, all distributions that result in reasonable fits to the observed spectrum exhibit maximum intensity near the same value of $g_\parallel$. The $g_\parallel$ values listed in Figures 1 and 3 and Table 1 are those obtained at the maximum. These values are accurate to ±0.001.

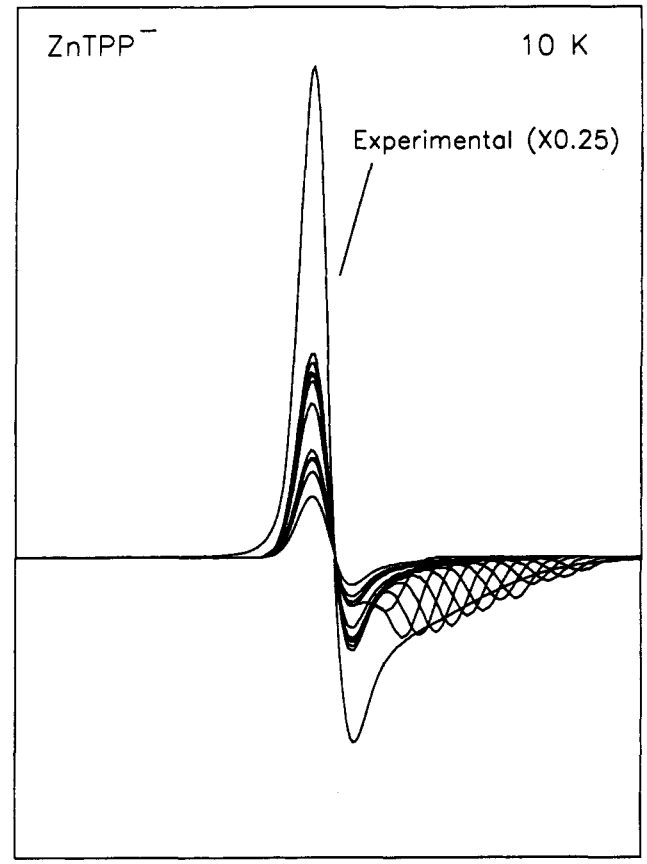

Figure 5. A distribution of $g_\parallel$ values that accounts for the broad $g_\parallel$ component of ZnTPP⁻ at 10 K. In the simulated spectrum, the different $g_\parallel$ features are located in the 1.9790–1.9985 range at increments of 0.0015; $g_\perp$ = 2.0034 for all the components. The intensities of the different $g_\parallel$ components were adjusted to fit the experimental spectrum. The line widths for the all the $g_\parallel$ and $g_\perp$ components are 2 G.

The EPR spectra of the different isotopomers of ZnTPP⁻ fail to reveal any resolved hyperfine structure at either ambient or low temperature (Figure 3). The ambient-temperature signal is sufficiently broad that the isotopic substitutions do not affect the width. On the other hand, isotope effects are clearly observed on the narrow $g_\perp$ feature in the low-temperature spectra. In particular, the $g_\perp$ signal for [ZnTPP-β-d_8]⁻ is distinctively

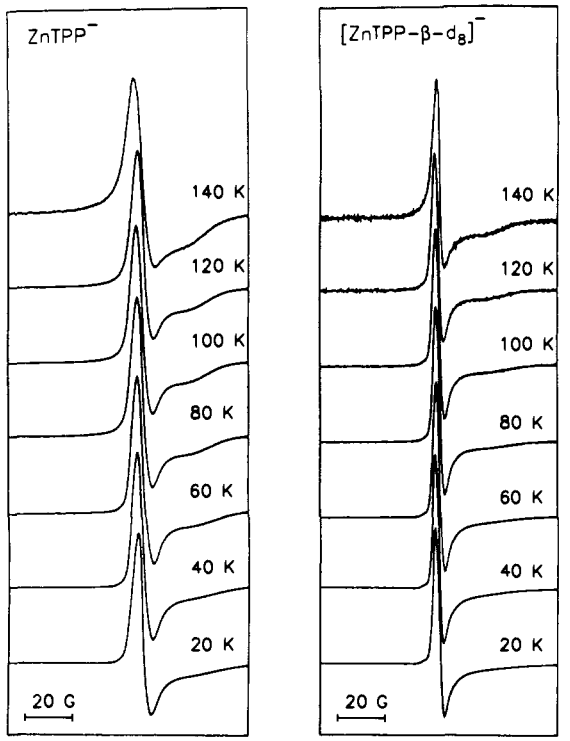

Figure 6. EPR spectra of electrochemically generated ZnTPP⁻ and [ZnTPP-β-d_8]⁻ in BuN in the 20–140 K range.

narrower than that for ZnTPP⁻, whereas the line width for [ZnTPP-(*meso*-^{13}C)$_4$]⁻ is significantly broader. In contrast, the line widths for the $g_\perp$ (and $g_\parallel$) signals of ZnTPP⁻ and [ZnTPP-($^{15}N_4$)]⁻ are essentially identical. Isotope effects are also observed on the broad $g_\parallel$ features of [ZnTPP-(*meso*-^{13}C)$_4$]⁻ and [ZnTPP-β-d_8]⁻. In the case of [ZnTPP-(*meso*-^{13}C)$_4$]⁻, $g_\parallel$ is broader than that of ZnTPP⁻, as is also observed for $g_\perp$. On the other hand, at 77 K, the $g_\parallel$ signal for [ZnTPP-β-d_8]⁻ is broader than that of ZnTPP⁻. At 10 K, the $g_\parallel$ feature of the deuteriated complex is so broad that it is barely observable (Figure 1). This result is opposite to that observed for the $g_\perp$ signals and opposite to that expected on the basis of the magnetogyric ratios of the two isotopes. Accordingly, these results indicate that the difference in line widths observed for the $g_\parallel$ signals of ZnTPP⁻ versus [ZnTPP-β-d_8]⁻ is not due to unresolved hyperfine structure. Spectral simulations indicate that a distribution with $g_\parallel$ components as low as 1.97 is needed to reproduce the high-field wing of the spectrum of [ZnTPP-β-d_8]⁻. This will be discussed further below. For all the isotopomers of ZnTPP⁻, the EPR spectra could be simulated by using the same hyperfine parameters as those obtained for H_2TPP⁻. The parameters reported for the β-hydrogen atoms of ZnTPP⁻ in Table 1 are half of those of H_2TPP⁻ because the symmetry of the former complex is assumed to be D_{4h} whereas the latter is D_{2h}. In the higher symmetry environment, all eight β-hydrogens are equivalent and contribute hyperfine structure to the band contour.

The anomalously broad $g_\parallel$ signal observed for [ZnTPP-β-d_8]⁻ versus ZnTPP⁻ prompted us to examine the temperature dependence of the EPR spectra of all four Zn(II) TPP-isotopomers in detail. The spectra observed for ZnTPP⁻ and [ZnTPP-β-d_8]⁻ in the 20–140 K range are compared in Figure 6. As is evident, the line widths for the $g_\parallel$ features of the two complexes are different at all temperatures. As the temperature is increased, the $g_\parallel$ feature of both anions appears to grow more intense. Similar behavior is observed for [ZnTPP-(*meso*-^{13}C)$_4$]⁻ and [ZnTPP-(^{15}N)$_4$]⁻ (not shown). At ~140 K, the intensity of the $g_\parallel$ signal observed for [ZnTPP-β-d_8]⁻ is approximately comparable to that observed for ZnTPP⁻ at ~80 K. These spectral changes were found to be completely reversible upon cycling the temperature over the 10–140 K range. Simulations of the spectra of both anions indicate that the temperature dependence can be modeled by using a distribution of $g_\parallel$ values in which the position of the maximum is approximately constant but whose width changes as a function of temperature. At all temperatures, the distribution for [ZnTPP-β-d_8]⁻ is skewed to lower g values than that for ZnTPP⁻.

In order to investigate whether the temperature dependent changes in the $g_\parallel$ signal could be attributed to population of a low-lying excited state(s), Curie plots were constructed at a number of resonance fields across the broad signal (not shown). These plots were consistent with all components of the signal arising from a single state. The power saturation behavior of the EPR signal was also investigated as a function of temperature. These studies indicate that all components of the $g_\parallel$ signal exhibit essentially identical saturation behavior. The saturation data provide further evidence that all components of the $g_\parallel$ signal are due to the same state. It should be noted, however, that the signals are difficult to saturate, even at low temperatures. At 77 K, no saturation effects are observed until powers exceed 100 mW. These data indicate that the spin relaxation rates for Zn(II) TPP⁻ are unusually fast. Collectively, the Curie plots and saturation data suggest that the temperature-dependent changes in the heterogeneous line width are determined by dynamical processes that modulate the parameters which determine $g_\parallel$ in the vibronic ground state. The fact that the spectral changes occur in the 20–140 K range suggests that the energy of the process is very low (50–100 cm^{-1}).

The temperature dependence of the EPR spectrum of ZnTPP⁻ in the 160–380 K range is shown in Figure 7. As the sample melts, the spectral features coalesce; however, the signal remains broad and asymmetric; the asymmetry is retained as the temperature is raised. Above 220 K, a new signal appears on the low-field side of the main signal. This feature grows with temperature and is quite apparent at 380 K. The new signal is indicated by an arrow in Figure 7. This arrow is positioned at $g = 2.02$; however, the exact position of the new signal is difficult to determine because it is extremely broad and overlaps with the principal spectral feature at $g_{av} \approx 2.00$. Regardless, it is clear that the g value of the new signal is higher than g_e. The fact that the new signal appears at elevated temperatures suggests that it is due to a thermally populated excited state. It is not possible to estimate the population of this state from the EPR signal because of its width and overlap with the signal at $g_{av} \approx 2.00$. Attempts to enhance the contribution of the low-field signal via power saturation were unsuccessful because the principal signal only begins to saturate at powers greater than 100 mW and does not completely saturate at the maximum power available from the microwave bridge. Regardless, the temperature range in which the low-field signal appears suggests that it is due to a state lying 100–300 cm^{-1} above the ground state. Finally, it should be noted that the spectral changes observed in the liquid state are completely reversible, as is the case for the spectral changes observed in the frozen samples (Figure 6).

3. CdTPP⁻. The EPR spectrum of CdTPP⁻ is different from that of the other three anions; however, its general characteristics are similar to those of ZnTPP⁻ (Figure 1). At ambient temperatures, the EPR signal from CdTPP⁻ is extremely broad (~120 G) and weak and is centered at $g_{av} = 1.995$. A much narrower signal (~5 G) at $g_{av} = 2.0026$ is superimposed on the broad signal. On the basis of its g value and line width, we attribute the narrow signal to the H_2TPP⁻ impurity formed during the reduction process (vide supra). In this regard, Felton and Linschitz have previously reported that CdTPP⁻ exhibits a narrow signal (~7 G) at $g_{av} = 2.0025$.[12] We believe that this signal may also be due to a H_2TPP⁻ impurity rather than to CdTPP⁻. At low temperatures, the line shape of CdTPP⁻ is distinctly anisotropic. The $g_\parallel$ signal is extremely broad, and simulations indicate that the maximum in the distribution of values is centered

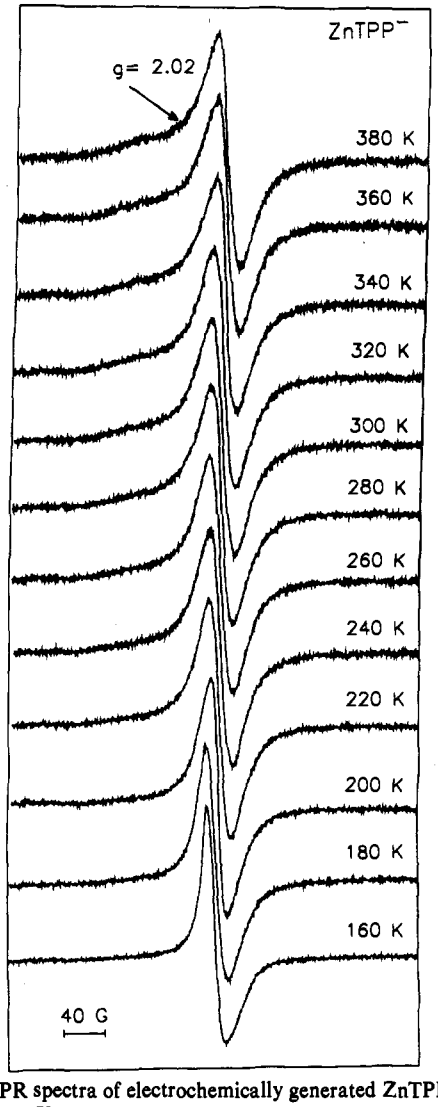

Figure 7. EPR spectra of electrochemically generated ZnTPP⁻ in BuN in the 160–380 K range.

near $g_{\parallel} \approx 1.980$. This value is lower than that observed for ZnTPP⁻ and is consistent with the observation that g_{av} for the ambient-temperature EPR signal of CdTPP⁻ is also lower than that of ZnTPP⁻ (Figure 1, Table 1).

B. OEP Complexes. EPR spectra were obtained for H_2OEP^-, $[H_2OEP\text{-}meso\text{-}d_4]^-$, ZnOEP⁻, and $[ZnOEP\text{-}meso\text{-}d_4]^-$ at ambient and low temperatures (77 K). These anions were generated electrochemically in BuN. A detailed investigation of the effects of solvent and counterion was not performed for the OEP anion radicals because the general characteristics of their ambient- and low-temperature spectra were found to be similar to those of the TPP analogs. The spectral parameters observed for the different OEP anions are summarized in Table 1.

At ambient temperatures, H_2OEP^- exhibits a narrow signal (5.8 G) at $g_{av} = 2.0027$ with no hyperfine structure (not shown). The signal observed for $[H_2OEP\text{-}meso\text{-}d_4]^-$ is significantly narrower (2.8 G) than that of H_2OEP^-, indicative of the unresolved *meso*-hydrogen atom hyperfine structure which contributes to the band contour of the normal isotopomer. At low temperatures, the EPR signals of both isotopomers are slightly anisotropic (not shown) as observed for H_2TPP^-. Simulations of the EPR spectra of H_2OEP^- and $[H_2OEP\text{-}meso\text{-}d_4]^-$ yielded hyperfine couplings for the *meso*-hydrogen atoms that are commensurate with a spin density on the *meso*-carbon atoms of ~0.1. This value is the same as that obtained directly from the *meso*-^{13}C hyperfine coupling in $[ZnTPP\text{-}(^{13}C)_4]^-$ (vide supra).

The ambient and low-temperature EPR spectra of ZnOEP⁻ and $[ZnOEP\text{-}meso\text{-}d_4]^-$ are shown in Figure 8. At ambient

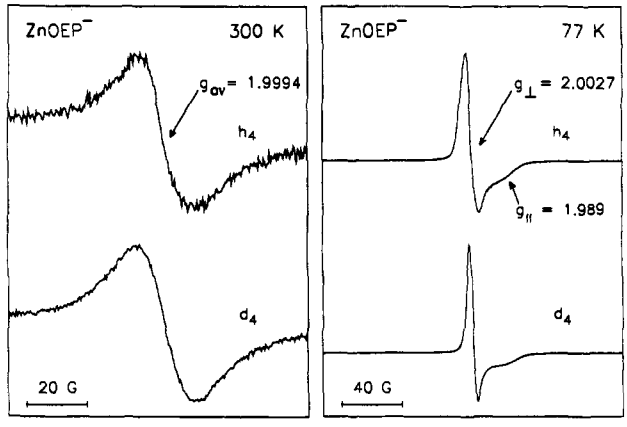

Figure 8. EPR spectra of electrochemically generated ZnOEP⁻ and $[ZnOEP\text{-}(meso\text{-}d_4)]^-$ in BuN at 300 and 77 K.

temperatures, the EPR signals from both complexes are broad (~18 G) and asymmetrical with $g_{av} < g_e$. At low temperatures, the signals are anisotropic with $g_{\perp} = 2.0027$ and $g_{\parallel} = 1.989$. The $g_{\perp}$ signal is narrow whereas the $g_{\parallel}$ signal is broad. No hyperfine structure is observed for either ZnOEP⁻ or $[ZnOEP\text{-}meso\text{-}d_4]^-$ at ambient or low temperatures. The line width for the ambient-temperature signal is not affected by isotopic substitution; whereas the line width for the low-temperature $g_{\perp}$ feature of the deuteriated complex is significantly narrower than that of the normal isotopomer. All of the above noted spectral characteristics for ZnOEP⁻ are similar to those observed for ZnTPP⁻. The EPR spectra of ZnOEP⁻ and ZnTPP⁻ do, however, differ in one significant respect. In the case of ZnOEP⁻, deuteriation at the *meso*-position narrows the $g_{\parallel}$ signal, as would be expected upon collapse of the hyperfine structure. This is apparent from inspection of Figure 8 (right panel). This behavior is in marked contrast to that observed for ZnTPP⁻, where deuteriation at the β-positions broadens the $g_{\parallel}$ signal. Simulations of the spectra indicate that distributions of $g_{\parallel}$ values with identical widths give reasonable fits to the spectra of both ZnOEP⁻ and $[ZnOEP\text{-}meso\text{-}d_4]^-$.

Discussion

The EPR data for the porphyrin anion radicals provide new insights into the characteristics of their electronic ground states. In particular, the anisotropy observed in the low-temperature spectra, as well as the low values of g_{av} observed for the Zn(II) and Cd(II) complexes at ambient temperatures, indicates that the orbital angular momentum is not completely quenched in the ^2E_g ground states of any of the metalloporphyrin anions. The deviations of $g_{\parallel}$ below g_e are due to the circulation of the unpaired electron in the e_g^* orbital of the macrocycle (for convenience we use this notation for the free bases). This motion gives rise to a component of angular momentum perpendicular to the plane of the ring.[19,28,29] The magnitude of the angular momentum is given by $i\Lambda = \langle e_{gx}|l_z|e_{gy}\rangle$. The value of $g_{\parallel}$ depends on both Λ and a matrix element of the form $Z = \lambda\Lambda$, where λ is the effective spin–orbit coupling. The observed $g_{\parallel}$ value is determined by these parameters as well as the magnitude of the Jahn–Teller and strain distortions.[28-30] These distortions alter vibronic interactions in the ^2E_g state. In the sections that follow, we first discuss the different factors that influence the value of $g_{\parallel}$. We then discuss the EPR data for porphyrin anion radicals in terms of a single-mode vibronic model that accounts for all the general features in the spectra. Finally, we discuss the effects of multimode Jahn–Teller activity on the detailed characteristics of the spectra.

(28) Canters, G. W.; van der Waals, J. H. In *The Porphyrins*; Dolphin, D., Ed.; Academic Press: New York, 1978; Vol. III, pp 531–582.
(29) van der Waals, J. H.; van Dorp, W. G.; Schaafsma, T. J. In *The Porphyrins*; Dolphin, D., Ed.; Academic Press: New York, 1978; Vol. IV, pp 257–312.
(30) Hoffman, B. M.; Ratner, M. A. *Mol. Phys.* **1978**, *35*, 901–925.

A. Factors Influencing $g_\parallel$. Molecular orbital calculations by McHugh and Gouterman predict that the intrinsic angular momentum associated with the e_g^* orbitals is $\Lambda \approx 2\hbar$ and that the magnitude of Λ is similar for both porphyrin dianions (D_{4h} symmetry) and free base porphyrins (D_{2h} symmetry).[31] In the case of transition metal porphyrins, the value of Λ is affected by mixing between the e_g^* and d_π orbitals of the metal ion. However, for closed-shell metals, such as Zn(II) and Cd(II), Ake and Gouterman have shown that the mixing is extremely small.[32] Calculations on Zn(II) porphyrins predict the coefficient to be 0.0242. The Z values for all of the porphyrin anion radicals are expected to be very small. In the case of the free base, only the carbon and nitrogen atoms in the ring contribute to Z. These atoms are also the only contributors to Z for the Mg(II) complex because there are no occupied metal orbitals of the appropriate symmetry to mix with the e_g^* orbitals of the macrocycle. Accordingly, the Z value for the Mg(II) complex is expected to be comparable to that of the free base. The Z values for the transition metal porphyrins are significantly larger due to mixing between the metal and porphyrin orbitals. In the case of Zn(II) porphyrins, Ake and Gouterman have calculated $Z \approx 0.7$ cm^{-1}.[32] Calculations have not been reported for Cd(II) porphyrins; however, on the basis of the larger spin–orbit coupling and increased extent of the 4d orbitals, Z would be estimated to be approximately twice that of the Zn(II) complexes.

The ^2E_g ground state of the metalloporphyrin anion radicals is subject to both static and dynamic Jahn–Teller effects.[1,19,28,29] The general consequences of Jahn–Teller instabilities in E states of systems with a 4-fold axis of symmetry have been examined in detail by several authors.[30,33–35] van der Waals and co-workers have extensively investigated the Jahn–Teller effect in the lowest lying E_u excited states of metalloporphyrins.[28,29] The reader is referred to these articles for a more complete discussion. The effect of a static Jahn–Teller distortion on a doubly degenerate harmonic potential is illustrated in Figure 9. The top curve represents the undistorted system. The middle curves represent the Jahn–Teller distorted system. The distortion displaces the two potentials by $\pm Q_0$ and lowers the energies of both by $E_{JT} = {}^1/_2 k Q_0^2$, where k is the force constant for the potential. The Jahn–Teller distortion affects the value of $g_\parallel$ by perturbing the Franck–Condon overlaps, $\langle i|j\rangle$, between the vibronic wave functions in the two potential wells. The displacement decreases the overlaps and scales the values of both Λ and Z ($\Lambda' = \langle i|j\rangle\Lambda$, $Z' = \langle i|j\rangle Z$).[28,30]

The Jahn–Teller active system is also subject to strain distortions which alter the relative energies of the two potentials with respect to one another.[28–30] The effect of strain is illustrated by the bottom curves in Figure 9, which shows the stabilization of one of the two Jahn–Teller distorted states by an amount δ. The energetic displacement of the two wells with respect to one another attenuates the orbital angular momentum and reduces the deviation of $g_\parallel$ from g_e. Strain distortions occur in the solid state because of crystal field effects or interactions with the solvent matrix. Spectroscopic studies on the lowest lying ^1E_u and ^3E_u excited states of metalloporphyrins have shown that strain in the solid state separates the two wells by as much as 100 cm^{-1}.[28,36] Interestingly, MCD studies of metalloporphyrins in solution indicate that the strain distortions in the liquid are comparable to those in the solid state.[37] The protonation of the pyrrole nitrogen atoms in free base porphyrins can be viewed as an intrinsic form of strain which distorts the molecule into a D_{2h} geometry. However, this strain energy is very large and separates the two wells by $\sim$3000 cm^{-1}.[19]

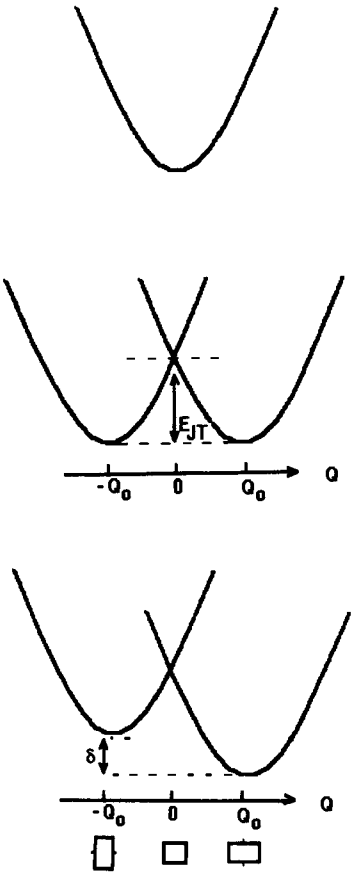

Figure 9. Effects of Jahn–Teller and strain distortions on an E state of a molecule with a 4-fold axis of symmetry. The top curve represents the undistorted system. The middle curves represent the Jahn–Teller distorted system. The distortion displaces the two potentials by $\pm Q_0$ and lowers the energies of both by $E_{JT} = {}^1/_2 k Q_0^2$. The bottom curves represents the effect of a strain distortion. Strain alters the relative energy of one well with respect to the other by an amount δ.

The $g_\parallel$ value can be used to obtain values of E_{JT} and δ, provided that reliable estimates for Λ and Z are available.[28] However, the solution of the Schrödinger equation for the dynamic Jahn–Teller system requires knowledge of all the vibronic interactions.[30,33–35] In the case of D_{4h}-symmetry metalloporphyrins, there are 18 modes of the basic ring skeleton (nine b_{1g}'s and nine b_{2g}'s) that are potentially Jahn–Teller active. These modes range in frequency from 150 to 1650 cm^{-1}.[38–42] In principal, the macrocycle can exhibit Jahn–Teller and strain distortions along each of these coordinates. At this time, there is relatively limited data concerning the extent of Jahn–Teller activity of the various modes. Resonance Raman studies of ZnTPP$^-$ have identified several high-frequency (1300–1600 cm^{-1}) modes that appear to be Jahn–Teller active.[38,42] Spectroscopic studies of the ^1E_u excited state of Zn(II) porphine indicate that a 180-cm^{-1} vibration is active in this state.[28,36] Collectively, these data suggest that a number of vibrations are Jahn–Teller active. If more than one or two vibrational modes exhibit significant Jahn–Teller activity, it is not likely that the values of E_{JT} and δ for every mode could be uniquely determined.

(31) McHugh, A. J.; Gouterman, M. *Theor. Chim. Acta* **1972**, *24*, 346–370.
(32) Ake, R. L.; Gouterman, M. *Theor. Chim. Acta* **1969**, *15*, 20–42.
(33) Child, M. S. *Mol. Phys.* **1960**, *3*, 601–603.
(34) Hougen, J. T. *J. Mol. Spectrosc.* **1964**, *13*, 149–167.
(35) Ballhausen, C. J. *Theor. Chim. Acta* **1965**, *3*, 368–374.
(36) Canters, G. W.; Jansen, G.; Noori, M.; van der Waals, J. H. *J. Phys. Chem.* **1976**, *80*, 2253–2259.
(37) Sutherland, J. C.; Axelrod, D.; Klein, M. P. *J. Chem. Phys.* **1972**, *54*, 2888–2898.
(38) Atamian, M.; Donohoe, R. J.; Lindsey, J. S.; Bocian, D. F. *J. Phys. Chem.* **1989**, *93*, 2236–2243.
(39) Li, X.-Y.; Czernuszewicz, R. S.; Kincaid, J. R.; Su, Y. O.; Spiro, T. G. *J. Phys. Chem.* **1990**, *94*, 31–47.
(40) Li, X.-Y.; Czernuszewicz, R. S.; Kincaid, J. R.; Stein, P.; Spiro, T. G. *J. Phys. Chem.* **1990**, *94*, 47–61.
(41) Perng, J.; Bocian, D. F. *J. Phys. Chem.* **1992**, *96*, 4804–4811.
(42) Reed, R. A.; Prendergast, K.; Purrello, R. A.; Spiro, T. G. *J. Phys. Chem.* **1991**, *95*, 9720–9727.

B. Single-Mode Vibronic Jahn–Teller Model. The limited amount of data available on the Jahn–Teller active vibrational modes precludes a detailed analysis of the EPR spectra of the porphyrin anion radicals. Nevertheless, insights can be gained into the factors affecting the ^2E_g ground state by examining the solution to the Schrödinger equation for the case of a single Jahn–Teller active mode. In the limit that Z is small compared to δ, the wave functions can be obtained from first-order perturbation theory.[28,30] This solution is appropriate for the porphyrin anions because $Z < 1$ cm^{-1} and the EPR data indicate that $\delta \geq 100$ cm^{-1} (vide infra). The perturbed wave functions can then be used to obtain $g_\parallel$ for both the ground state and the low-lying excited state δ cm^{-1} above the ground state. The $g_\parallel$ values for the lowest vibrational levels of these two states are given by

$$g_\parallel = g_e \mp \frac{2Z\Lambda\sum_v |\langle 0|v\rangle|^2}{\delta \pm v\bar{\nu}} \quad (1)$$

where the upper and lower signs refer to the ground and excited states, respectively, v are the vibrational quantum numbers, $\bar{\nu}$ is the vibrational frequency of the Jahn–Teller active mode, and the definitions of the Z, Λ, and δ are the same as those previously given.[30] The Franck–Condon factors are related to the displacement along the Jahn–Teller active vibrational coordinate by

$$|\langle 0|v\rangle|^2 = \frac{S^v}{v!}e^{-S} \quad (2)$$

where $S = 2\tilde{Q}_0^2$ and $\tilde{Q}_0$ is the displacement in dimensionless coordinates.[43] The value of E_{JT} depends on the vibrational frequency of the Jahn–Teller active mode and is related to S by $E_{JT} = S\bar{\nu}/4$.[28,30,33–35] The $g_\parallel$ values for the vibrationally excited states can also be obtained from eq 1 by substituting the appropriate Franck–Condon factors and adding a term to the denominator to account for the energy of the vibrational excitation.[28] [It should be noted that eq 1 breaks down when the vibronic levels of the upper and lower wells are accidentically degenerate.]

All of the general features observed in the low-temperature EPR spectra of the porphyrin anion radicals can be accounted for with eq 1. In the case of H_2TPP^- and H_2OEP^-, Z is extremely small and δ is large. The combination of these factors results in a very small shift of $g_\parallel$ from g_e ($\sim$0.0003). The Z value for $MgTPP^-$ is comparable to that of the free base; however, δ is much smaller. The smaller strain energy results in a clearly observable deviation of $g_\parallel$ from g_e ($\sim$0.0023). The δ values for $ZnTPP^-$, $ZnOEP^-$, and $CdTPP^-$ are expected to be similar to those of $MgTPP^-$; however, the Z values of the former complexes are much larger than those of the latter [$Z(CdTPP^-) > Z(ZnTPP^-) \sim Z(ZnOEP^-) \gg Z(MgTPP^-)$]. The large Z values for the Zn(II) and Cd(II) complexes result in significant deviations of $g_\parallel$ from g_e ($\sim$0.01 and $\sim$0.02, respectively).

The Jahn–Teller and strain parameters for the Zn(II) and Cd(II) porphyrin anion radicals can be estimated from eqs 1 and 2. In the case of the Zn(II) anions, the calculations indicate that the upper bounds for S and δ are 2.5 and 250 cm^{-1}, respectively. This is illustrated in Table 2, which lists the $g_\parallel$ values calculated for S and δ in the ranges 0–2.5 and 10–250 cm^{-1}, respectively. The calculations were performed by using the values $\Lambda = 2\hbar$ and $Z = 0.7$ cm^{-1}, which were determined for Zn(II) porphyrins by Gouterman and co-workers.[31,32] The vibrational frequency of the Jahn–Teller active mode was assumed to be 1000 cm^{-1}, which is in the range observed in resonance Raman studies of $ZnTPP^-$.[38,42] Inspection of Table 2 reveals that there are a number of combinations of S and δ that give $g_\parallel$ values in accord with those observed for $ZnTPP^-$ and $ZnOEP^-$. The $g_\parallel$ values listed in boldface correspond to the values calculated for a given value of S and δ that are closest to those observed (Table 1). The lower $g_\parallel$ values observed for $CdTPP^-$ can also be accounted for by the range of S and δ values listed in Table 2, assuming that Z for this complex is approximately twice as large as that of the Zn(II) anions.

Table 2. Effects of Jahn–Teller and Strain Distortions on the $g_\parallel$ Values[a]

	δ					
S[b]	10	50	100	150	200	250
0	1.7223	1.9463	1.9743	1.9836	**1.9883**	**1.9911**[c]
0.25	1.7837	1.9581	1.9800	1.9873	1.9909	1.9931
0.50	1.8315	1.9674	1.9844	**1.9901**	1.9930	1.9947
0.75	1.8688	1.9747	**1.9880**	1.9924	1.9947	1.9960
1.00	1.8979	1.9804	1.9907	1.9942	1.9960	1.9971
1.25	1.9207	1.9849	1.9930	1.9957	1.9971	1.9979
1.50	1.9384	**1.9884**	1.9947	1.9968	1.9979	1.9986
1.75	1.9522	1.9912	1.9961	1.9978	1.9986	1.9991
2.00	1.9630	1.9934	1.9972	1.9985	1.9992	1.9996
2.25	1.9715	1.9951	1.9981	1.9991	1.9996	2.0000
2.50	1.9780	1.9965	1.9988	1.9996	2.0000	2.0003

[a] Values calculated using eq 1 with Λ 2.0$\hbar$, $Z = 0.7$ cm^{-1}, and $\bar{\nu} = 1000$ cm^{-1} (see text). [b] $S = 2\tilde{Q}_0^2$. [c] Values in bold are those closest to the $g_\parallel$ values observed for the Zn(II) anion radicals at 77 K.

In order to narrow the range of S and δ, an independent measure is needed for one of the two parameters. The temperature-dependent EPR data provide some additional insight into the possible values of δ. In particular, no signals attributable to the upper state of the Jahn–Teller system are observed in the 10–140 K range. This state is characterized by a $g_\parallel$ value greater than g_e when $\bar{\nu} \gg \delta$ (eq 1). To a first approximation, $g_\parallel$ for the upper state should deviate from g_e by an amount similar to that of $g_\parallel$ for the ground state. It is possible that the EPR signal from the upper state is extremely broad due to fast relaxation processes; however, the baseline on the low-field side of g_e shows no inflections that suggest an underlying broad signal. The EPR spectra obtained in the 160–220 K range also fail to exhibit any sign of new signals (Figure 7). In the liquid state, the signals from the upper state would be more difficult to identify because the g_{av} values for both the lower and upper states collapse toward g_e. Nevertheless, a weak broad signal is clearly present at elevated temperatures (300–380 K). The fact that g_{av} for this signal is above g_e strongly suggests that it is due to the upper Jahn–Teller state. Determination of the population of this state would provide a direct measure of δ. However, as was previously noted, the width of the lower-field EPR signal and its overlap with the principal signal preclude any accurate evaluation of their relative intensities. Regardless, it seems reasonable that the thermally populated state must be at least 100 cm^{-1} above the ground state. If the minimum value of δ is assumed to be 100 cm^{-1}, S is constrained to be less than unity (Table 2) and E_{JT} is less than 250 cm^{-1} (assuming $\bar{\nu} = 1000$ cm^{-1}). It should be noted that if $\bar{\nu}$ and δ are comparable, then $g_\parallel$ is strongly dependent on the vibrational quantum number. In this case, excited vibrational levels of the lower electronic state can exhibit $g_\parallel > g_e$ and the lowest vibrational level of the upper electronic state can exhibit $g_\parallel < g_e$. Therefore, it is possible that the signal with $g_{av} > g_e$ is due to a thermally populated vibrational level of a low-frequency Jahn–Teller active mode in the ground electronic state.[28,36] Even if this is the case, calculations indicate that the δ and S values are constrained to the same range as that noted above.

For an S less than unity, the zero point energy of any Jahn–Teller active vibrational mode is necessarily greater than E_{JT}. Accordingly, the Jahn–Teller distortion in the metalloporphyrin anion radicals is dynamic rather than static in nature. [A static distortion occurs when the zero point energy is less than E_{JT}, which is only possible for $S > 2$ because $E_{JT} = S\bar{\nu}/4$.] The dynamic distortion averages the structure of the molecule. However, the fact that δ is non-negligible indicates that the dynamically averaged structure does not have 4-fold symmetry. The average

(43) Manneback, C. *Physica* **1951**, *17*, 1001–1010.

deviation from 4-fold symmetry depends on the magnitude of $\bar{\nu}$ versus δ. The asymmetry along the coordinates of high-frequency vibrational modes should be relatively small.[38,42] On the other hand, the asymmetry could be pronounced along the coordinates of low-frequency modes.[28,36] In this regard, the $\bar{\nu}$'s of only one or two of the 18 potentially Jahn–Teller active modes of metalloporphyrins lie in the range of δ's obtained from analysis of the EPR data.[39,40]

C. Effects of Multimode Jahn–Teller Activity. As was previously noted, resonance Raman studies of ZnTPP$^-$ indicate that several vibrational modes are Jahn–Teller active.[38,42] In addition, the detailed features observed in the EPR spectra of the Zn(II) and Cd(II) anions are highly suggestive of multimode vibronic activity (vide infra). Consequently, the question arises whether multimode effects significantly alter the picture of the Jahn–Teller and strain distortions drawn on the basis of the single-mode vibronic model. The consequences of multimode Jahn–Teller activity in the E state of systems with a 4-fold axis of symmetry have not been examined in general; however, Hoffman and Ratner have investigated the case of two Jahn–Teller active modes which are subject to strain distortions.[30] When the strain energy is non-zero along both of the vibronically active coordinates, the minima on the potential surface occur approximately along the coordinate with the largest Jahn–Teller activity provided that the strain energy along this coordinate is comparable to or greater than the strain along the less active coordinate. As the strain along the latter coordinate increases, the potential minima distort and then shift such that the displacement is along both vibronically active coordinates. When the strain along the less active coordinate is significantly greater than that along the more active coordinate, the potential minima occur along the former coordinate.

The detailed characteristics of a potential surface with more than two Jahn–Teller active modes are not easily visualized. Such a surface could exhibit a variety of features depending on the E_{JT} and δ values along the different coordinates. Nevertheless, the EPR data along with the predictions of the two-dimensional case provide some insights. In particular, the EPR data suggest that the minimum on the upper Jahn–Teller surface lies at least 100 cm^{-1} above that of the lower surface. These data also indicate that the ground state has appreciable unquenched orbital angular momentum. In any model, this precludes there being extremely large Jahn–Teller and/or strain distortions along a particular coordinate. The energetic displacement of the excited state also defines an *approximate* upper bound for the strain energy along any particular coordinate regardless of whether this coordinate exhibits the largest Jahn–Teller activity. This upper bound is only approximate because the exact position of the minima depends on the relative values of E_{JT} and δ for the various modes.[30] Given the $g_\parallel$ values observed for the Zn(II) and Cd(II) porphyrin radical anions and by presuming that the calculated values of Z and Λ are accurate, it is unlikely that the δ values for any vibrational mode could fall outside the range listed in Table 2.

On a multidimensional harmonic potential surface, the total Franck–Condon overlap is determined by the product of the overlaps of the individual modes and the total S is equal to the sum of the S values for the individual modes. When the total S for the multimode harmonic oscillator equals the S of a one-dimensional oscillator, the net Franck–Condon overlaps are identical. Accordingly, the S value obtained from the single-mode vibronic model can be viewed as an effective S. For modes with $\bar{\nu} \gg \delta$ ($\bar{\nu}$ in the 500–1650-cm^{-1} range), the effective S represents an upper bound for the individual S values. Consequently, the S values for these modes must fall within the range shown in Table 2. For very low frequency modes, it is possible that the S values could exceed those shown in Table 2; however, the E_{JT}'s must be sufficiently small that the lowest energy minima on the potential surface do not occur along these coordinates. If E_{JT} (and S) along one of these coordinates were sufficiently large to result in such minima, then δ would necessarily be very small (Table 2). This is not compatible with the 100-cm^{-1} splitting between the upper and lower Jahn–Teller states. Collectively, the above arguments suggest that explicit consideration of multimode Jahn–Teller activity would not significantly alter the general picture of the Jahn–Teller and strain distortions derived from the single-mode vibronic model.

Although the single-mode model accounts for the general features of the EPR signals of the metalloporphyrin anion radicals, multimode effects do appear to influence the detailed characteristics of the signals. In particular, these effects probably give rise to the distribution of $g_\parallel$ values observed in the low-temperature EPR spectra of the Zn(II) and Cd(II) complexes. On the multidimensional potential surface there could be a number of nearly isoenergetic forms with different effective S values. There is no a priori reason to expect that these S values would be randomly distributed. This would lead to a non-Gaussian distribution of $g_\parallel$ values as is observed (vide supra). [A random distribution of S values should result in a Gaussian distribution of $g_\parallel$ values because $g_\parallel \propto S$ (eq 1).] If the potential surface is soft along a number of coordinates, the $g_\parallel$ value would also be very sensitive to strain effects. In general, the distribution of strain energies is expected to be random. However, a random distribution of δ values results in an intrinsically non-Gaussian distribution of $g_\parallel$ values because $g_\parallel \propto \delta^{-1}$. In this regard, we initially attempted to model the low-temperature EPR spectra by assuming a Gaussian distribution of δ values. Although this model gives a better fit to the observed spectra than do simulations performed with a Gaussian distribution of S values, the fit is not satisfactory. Collectively, these results suggest the distribution of $g_\parallel$ values is determined by the complicated interplay of a number of factors.

As the temperature is increased, the distribution of $g_\parallel$ values appears to narrow (Figure 6). This narrowing is most likely due to the modulation of the δ and S values by interactions with lattice phonons. Above the melting point of the solid matrix, the signal remains broad and asymmetric. The shape of this signal indicates that there is a nonrandom distribution of g_{av} values. In addition, the value of g_{av} measured at the zero crossing point in the solution spectra is very close to that obtained by averaging the values of $g_\perp$ and $g_\parallel$ observed in the low-temperature spectra (taking $g_\parallel$ as the maximum in the distribution). These data indicate that the average δ and S values in the liquid state are not substantially different from those in the solid matrix. If these values were different, then g_{av} should be different from the average of $g_\perp$ and $g_\parallel$. The fact that δ is relatively large in solution is consistent with the results of MCD experiments on the ^1E_u excited state of metalloporphyrins.[37] At elevated temperatures, other factors may also contribute to the distribution of $g_\parallel$ values that determines the EPR line shape. If low-frequency vibrational modes are Jahn–Teller active,[28,36] then excited vibrational levels of these modes can become populated at higher temperatures. The difference in $g_\parallel$ values together with the difference in populations of the ground and excited vibrational states could contribute to the asymmetry of the EPR signal. It is likely that all of the above factors influence the EPR line shape observed at elevated temperatures. The complications arising from multimode effects make a detailed analysis of the line shape extremely difficult.

One final point concerns the nature of the Jahn–Teller active vibrations in metalloporphyrin anion radicals. The observation that β-deuteriation alters the $g_\parallel$ values of ZnTPP$^-$ provides additional insight in this regard. In particular, the isotope sensitivity of the $g_\parallel$ values suggests that at least one Jahn–Teller active mode exhibits a substantial deuteriation shift. In a one-dimensional harmonic approximation, the deuteriation-induced downshift of the energy levels decreases the Frank–Condon

overlaps. This is equivalent to increasing the displacement along the dimensionless coordinate (larger S value). The larger S value for the deuteriated isotopomer would result in a $g_\parallel$ closer to g_e (eq 1). The observation that β-deuteriation of ZnTPP$^-$ shifts $g_\parallel$ further from g_e indicates that the effective S value is in fact decreasing. The smaller S value reflects the multimode nature of the vibronic interactions. In a multidimensional oscillator, isotopic substitution can significantly alter the forms of the vibrational eigenvectors.[38-40] These changes in the eigenvectors alter the relative S values for the different modes. The S value for a given mode can either increase or decrease.

The only vibrational modes of ZnTPP$^-$ that exhibit large β-deuteriation shifts are the β-hydrogen in-plane deformations ($\delta C_\beta H$) which are observed in the 1050–1200-cm^{-1} range.[38,39] Of these modes, two are potentially Jahn–Teller active, a 1080-cm^{-1} b_{1g} vibration and 1200-cm^{-1} b_{2g} vibration. Resonance Raman studies on ZnTPP and ZnTPP$^-$ indicate that b_{1g} vibrations exhibit the largest Jahn–Teller activity for the anion.[38] A number of b_{1g} vibrations, including the $\delta C_\beta H$ mode, appear to be Jahn–Teller active; however, the activity is particularly strong for the $\nu C_\beta C_\beta$ and $\nu C_\alpha C_m$ stretching vibrations of the ring. This latter observation is consistent with molecular orbital calculations on metalloporphyrin anion radicals which predict that the complex experiences a b_{1g} distortion along the $C_\beta C_\beta$ and $C_\alpha C_m$ bonds.[44] It would not normally be expected that large Jahn–Teller distortions would occur along the $C_\beta C_\beta H$ coordinate (the molecular orbital calculations are not sufficiently accurate to address this issue). However, normal coordinate calculations on metallo-TPP complexes indicate that the $\delta C_\beta H$ vibration is significantly mixed with the $\nu C_\beta C_\beta$ vibration observed near 1500 cm^{-1}.[38,39] This mixing is probably the origin of the Jahn–Teller activity for the former mode. The normal coordinate calculations also indicate that β-deuteriation significantly alters the extent of mixing and the form of the vibrational eigenvector of the deformation. This would alter the effective S value and could account for the anomalous β-deuteriation effects observed in the EPR spectra of ZnTPP$^-$. Mode mixing can also account for the absence of an anomalous *meso*-deuteriation effect in the spectra of ZnOEP$^-$. The EPR data indicate that none of the Jahn–Teller active modes exhibit large deuteriation shifts. The only candidate for such a mode is the b_{1g} $\delta C_m H$ vibration near 1220 cm^{-1}.[40] This deformation could only gain significant Jahn–Teller activity by mixing with the b_{1g} $\nu C_\alpha C_m$ mode near 1600 cm^{-1}. However, normal coordinate calculations on metallo-OEP complexes indicate that the mixing between the $\nu C_\alpha C_m$ and $\delta C_m H$ vibrations is relatively small.[40]

(44) Prendergast, K.; Spiro, T. G. *J. Phys. Chem.* **1991**, *95*, 9727–9736.

Summary and Conclusions

The EPR spectra of H_2TPP^-, H_2OEP^-, $MgTPP^-$, $ZnTPP^-$, $ZnOEP^-$, and $CdTPP^-$ have been obtained under a variety of conditions. Contrary to previous reports, the spectra are not particularly sensitive to the solvent or counterion. The low-temperature spectra of all the anion radicals are anisotropic with $g_\parallel < g_e$. The anisotropy for H_2TPP^- (and H_2OEP^-) and $MgTPP^-$ is small ($\sim$0.0003 and $\sim$0.0023, respectively). On the other hand, the anisotropy is significant for $ZnTPP^-$ (and $ZnOEP^-$) and $CdTPP^-$ ($\sim$0.01 and $\sim$0.02, respectively). The spectra have been modeled by using an harmonic potential function which is subject to both Jahn–Teller and strain distortions. The general characteristics of the spectra are well accounted for by a model that assumes a distortion along a single vibronically active coordinate. However, the detailed characteristics of the EPR line shape indicate that more than one mode is involved. Simulations of the anisotropic spectra indicate that E_{JT} is less than the zero point energy of the active vibrational modes; accordingly, the distortion is dynamic rather than static. The calculations, in conjunction with the spectral data, indicate that the strain energy is substantial (at least 100 cm^{-1}) in both the solid and liquid states. The strain distortion alters the relative energies of the two wells in the Jahn–Teller distorted system. Accordingly, the dynamically averaged structure does not have rigorous 4-fold symmetry.

Acknowledgment. We thank Drs. J. S. Lindsey and R. W. Wagner for the generous gift of the TPP isotopomers. This work was supported by Grant GM36243 (D.F.B.) from the National Institute of General Medical Sciences.